PERGAMON

Electrochimica Acta 48 (2002) 113–118

ELECTROCHIMICA Acta

www.elsevier.com/locate/electacta

Corrosion and passivation behaviors of some stainless steel alloys in molten alkali carbonates

A.A. Attia [a,*], S.A. Salih [b], A.M. Baraka [b]

[a] Chemistry Department, Faculty of Science, Zagazig University, Zagazig, Egypt
[b] Chemistry Department, Faculty of Science, Cairo University, Cairo, Egypt

Received 25 May 2002; received in revised form 28 June 2002; accepted 1 August 2002

Abstract

The corrosion and passivation behaviors of two types of stainless steel alloys (ferritic and austenitic steels) in ternary molten Li_2CO_3–Na_2CO_3–K_2CO_3 mixture at different temperatures (475–550 °C) were studied using galvanostatic polarization and cyclic voltammetry. The galvanostatic polarization curves of the investigated alloys illustrate the passivation and passivity breakdown of the alloys. The passivation potential range for the three investigated steel alloys is about 1.15–1.3 V. During this potential range different oxide and spinels are formed, the nature of which depends on the type of alloy and the anodization potential. At high anodic potentials the decomposition of carbonate takes place, leading to passivity breakdown and oxygen evolution. The values of corrosion parameters (R_p, i_o and i_{corr}) were calculated. The calculated values indicate that the corrosion resistance of the austenitic stainless steel is higher than that of the ferritic steel. The activation energy of the corrosion process was found to be equal to about 70 kJ mol^{-1}. The results of the cyclic voltammetric investigations indicate that the behavior of the austenitic steels is about the same and differs from that of ferritic steel. The corrosion tests in 0.2 M HCl solutions have shown that the oxide scales formed on the surface of the austenitic stainless steels are multilayered, whereas those formed on the ferritic alloy are uniform.

Keywords: Molten alkali carbonates; Corrosion; Passivation; Polarization; Stainless steel

1. Introduction

Fused salts are considered now as an accepted medium in many industrial processes. In the last decades more interest is devoted to the chemistry of fused salts [1]. They have been applied as coolants in nuclear reactors, heat transfer processes and as reaction media in chemical [2] and electrochemical processes [3]. They meet the requirements of many energy conversion processes, especially in fuel cell applications [4–8]. Molten alkali carbonates have drawn the attention of many research groups because of their useful applications in the environmentally safe fuel cells [8,9] and the recent developments including fuel recovery such as hydrogen, methane and other hydrocarbons from natural bio-compounds. In such applications, potentially corrosive compounds are formed and conditions for increased rates of corrosion are present [10,11].

Material degradation as a result of corrosion reactions is an important issue in energy production and energy consumption devices, especially current collectors and other metallic components of fuel cells [5–7,10,11]. Reactions between alloys and molten carbonates are technologically important in view of long term stability of molten carbonate fuel cells, which are under continuous development. Particular interest was paid to the corrosion processes occurring at the current collectors and steel parts of the fuel cell construction.

The corrosion behavior of stainless steel in molten alkali carbonate was the subject of many investigations, especially under the operation conditions of molten carbonate fuel cells [5,8,11–13]. The ternary alkali mixture Li_2CO_3–Na_2CO_3–K_2CO_3 represents a promising mixture because of its relatively low melting point (397 °C) and good electrical characteristics [14].

* Corresponding author. Tel.: +20-2-5676-558
E-mail address: wbadawy@main-scc.cairo.com (A.A. Attia).

0013-4686/02/$ - see front matter © 2002 Published by Elsevier Science Ltd.
PII: S0013-4686(02)00506-6

In the present investigation, the corrosion and passivation behaviors of two types of stainless steel in such ternary molten alkali carbonate mixture were studied. In this respect, galvanostatic polarization and cyclic voltammetry techniques have been employed. The oxide scales formed on the steel surface during its anodic oxidation in the carbonate melt have been analyzed, and the experimental results were discussed.

2. Experimental

Three specimens of the two types of stainless steel have been prepared and used in these investigations. The first is from ferritic steel with 15.05% Cr. The other two are from austenitic steel, one with 17.9% Cr+7.08% Ni and the other with 20.45% Cr+8.3% Ni.

The ternary molten mixture consists of pure lithium carbonate (Li_2CO_3), sodium carbonate (Na_2CO_3) and potassium carbonate (K_2CO_3) in a molar ratio of 43.5:31.5:25.0 mol%, respectively.

The carbonate mixture was placed in a special container in an electrically heated furnace where it is melted at 550 °C. The traces of humidity in the mixture were removed by bubbling dry CO_2 gas in the melt for 2 h. The mixture was left to cool in a dry atmosphere and the solidified mass was crushed and kept in a closed desiccator ready for use. In each experiment 50.0 g of the prepared ternary mixture was used.

The electrochemical cell consists of a Pyrex glass tube of 100 ml capacity in which the electrolyte (melt) and the electrodes were placed. The whole tall tube was placed in an outer cylindrical closed end alumina crucible of 500 ml capacity. The system was rendered gas tight using an O-ring seal between the outer alumina crucible and a stainless steel header in which the electrodes were fixed. The whole system was heated to the experimental temperature in an electrically heated vertical tube furnace. A Ni/Ni–Cr thermocouple, which was contained in a special tube to separate it from the melt, and a temperature indicator have been used for the temperature control.

The stainless steel working electrode were cut from both the ferritic and austenitic steel samples, as sheets of 1×1 cm^2 area and 0.1 cm thickness,. Each electrode was provided with a side 20 cm long and 0.2 cm width arm of the same material covered with a Pyrex glass tube of suitable diameter. The Pyrex tube was fused at the lower end directly attached to the square working area and sealed at its upper end by a suitable epoxy leaving an electrical contact.

Before each experiment, the electrode was abraded by emery papers of different grades down to 4/0, degreased with acetone and then immersed quickly in the melt. In each experiment a new steel electrode was used.

The potential of the working electrode was measured against a Ag/AgCl/Cl^- electrode which was accepted as a suitable reference electrode for such media [15–17] by means of D.C. microvoltmeter. The cyclic voltammetric measurements and the polarization experiments have been performed using the IM5D (Zahner Elektrik-GmbH) impedance system.

3. Results and discussion

The investigated specimens will be denoted hereafter as SI, SII and SIII for the ferritic (15.05% Cr) austenitic (17.9% Cr+7.08% Ni) and austenitic (20.45% Cr+8.3% Ni) steels, respectively.

3.1. Anodic polarization

In this series of experiments the anodic oxidation of the steel electrodes in the molten carbonate mixture at different working temperatures, 475, 500, 525 and 550 °C was investigated. In each experiment the electrode was immersed in the melt at the specified temperature and the potential was traced with time until a steady-state was achieved. The electrode was then polarized galvanostatically by applying a constant current for a fixed interval of 2 min. The potential corresponding to each polarization condition was measured and then the polarizing current was increased.

The corrosion parameters of each steel alloy were calculated from the galvanostatic polarization curves and presented collectively in Table 1. In this table, E_{pn}, represents the passivation potential of the steel alloy, which is considered to be the open circuit steady-state potential corresponding to the onset of passivity. E_b represents the passivity breakdown potential, R_p is the polarization (corrosion) resistance, i_o is the exchange current density and i_{corr} is the corrosion current density.

From the data presented in Table 1, it is clear that the passivation potential range, E_b–E_{pn}, for the three investigated steel alloys is about 1.15–1.3 V. During this potential range, it was assumed that different oxides and spinels are formed on the alloy surface. The nature of the formed material depends on the nature of the steel and its potential [18]. The anodic oxidation and scale formation proceeds according to different electrochemical reactions occurring between the alloy components and the carbonate melt under the experimental conditions according to the followimg scheme:

$$Cr + Li^+ + 2CO_3^{2-} \rightarrow LiCrO_2 + 2CO_2 + 3e \quad (1)$$

$$Fe + CO_3^{2-} \rightarrow FeO + CO_2 + 2e \quad (2)$$

$$Fe + Li^+ + 2CO_3^{2-} \rightarrow LiFeO_2 + 2CO_2 + 3e \quad (3)$$

These reactions lead to the formation of $LiCrO_2$, $LiFeO_2$ and FeO. FeO is unstable and oxidises further

Table 1
Corrosion parameters for the stainless steel alloys in carbonate melt at different temperatures

Alloy	Temperature (°C)	E_{pn} (mV)	E_b (mV)	$E_b - E_{pn}$ (mV)	R_p (O)	i_o (μA cm^{-2})	i_{corr} (μA cm^{-2})
	475	−1202	−50	1152	376	57.0	120
SI	500	−1277	−70	1157	257	86.2	150
	525	−1248	−80	1168	198	115.5	200
	550	−1277	−90	1187	119	198.3	350
	475	−1416	−200	1216	897	23.8	50
SII	500	−1438	−238	1200	553	40.1	65
	525	−1460	−245	1215	358	63.9	90
	550	−1468	−253	1215	262	90.1	150
	475	−1406	−196	1210	878	24.4	40
SIII	500	−1409	−119	1290	584	37.9	70
	525	−1412	−205	1207	401	57.1	80
	550	−1432	−198	1234	303	77.9	120

to Fe_3O_4 and Fe_2O_3 according to the following reactions:

$$3FeO + O^{2-} \rightarrow Fe_3O_4 + 2e \quad (4)$$

$$2Fe_3O_4 + O^{2-} \rightarrow 3Fe_2O_3 + 2e \quad (5)$$

At higher polarization, $LiCrO_2$ and also Cr itself undergo further oxidation to chromates which dissolve in the melt according to:

$$LiCrO_2 + 2CO_3^{2-} \rightarrow CrO_4^{2-} + 2CO_2 + Li^+ + 3e \quad (6)$$

$$Cr + 4CO_3^{2-} \rightarrow CrO_4^{2-} + 4CO_2 + 6e \quad (7)$$

The increase of the anodic potential enhances the formation of $LiFe_5O_8$ and the formation of α-Fe_2O_3 according to:

$$LiFeO_2 + 4Fe + 6CO_3^{2-} \rightarrow LiFe_5O_8 + 6CO_2 + 12e \quad (8)$$

$$2Fe + 3O^{2-} \rightarrow Fe_2O_3 + 6e \quad (9)$$

The austenitic stainless steel alloys SII and SIII are characterized by the formation of NiO according to:

$$Ni + CO_3^{2-} \rightarrow NiO + CO_2 + 2e \quad (10)$$

The formation of chromate, CrO_4^{2-}, has been identified in the chromium corrosion in carbonate melts [12]. In the case of pure chromium no transport problems are expected since lithium ions are available at the oxide/electrolyte interface so that the chromate ion can be easily formed and dissolved in the melt. In the case of steels and nickel-base alloys, the presence of mixed oxides causes transport problems which delay the chromate ion formation.

It should be noted that the oxygen ions, O^{2-}, required to induce reactions (4), (5) and (9) are produced as a result of carbonate decomposition at the melting temperature according to:

$$CO_3^{2-} \rightleftharpoons CO_2 + O^{2-} \quad (11)$$

At higher anodic potential, this decomposition reaction leads to a passivity breakdown and oxygen evolution according to the following reaction:

$$CO_3^{2-} \rightleftharpoons CO_2 + 1/2\ O_2 + 2e \quad (12)$$

The values of the polarization resistance, R_p, and the exchange current density, i_o, for the corrosion of the three specimens of the investigated stainless steels were calculated from the linear polarization of the alloy according to:

$$R_p = \frac{\Delta E}{\Delta i} = \frac{RT}{zF} \cdot \frac{1}{i_o} \quad (13)$$

where $\Delta E/\Delta i$ represent the slope of the potential versus current relation near the equilibrium potential, z is the number of electrons involved in the corrosion reaction which was taken as 3. R, T and F have their usual meanings. The values of the corrosion current density, i_{corr}, were calculated from the results of the polarization experiments.

Inspection of the values of the corrosion parameters presented in Table 1 shows that the corrosion resistance of the investigated steel alloys in the carbonate melt and hence their passiviation susceptibility is relatively high for the austenitic steel (SII and SIII) which contains both Cr and Ni beside Fe. It is more than twice the value of the corrosion resistance of the ferritic steel (SI). The polarization curves of the different alloys indicate that the corrosion process is accompanied by charge transfer overpotential, i.e. it is of the activation type [19]. The activation energy of the corrosion process was obtained from the linear variation of the rate of the corrosion reaction assigned as the corrosion current density, i_{corr}, with the temperature, which obeys the familiar Arrhenius equation [20]. This linear relation is represented as:

$$\frac{d \log i_{corr}}{d\left(\frac{1}{T}\right)} = \frac{E_a}{2.303R} \quad (14)$$

The linear plots of the three investigated alloys are

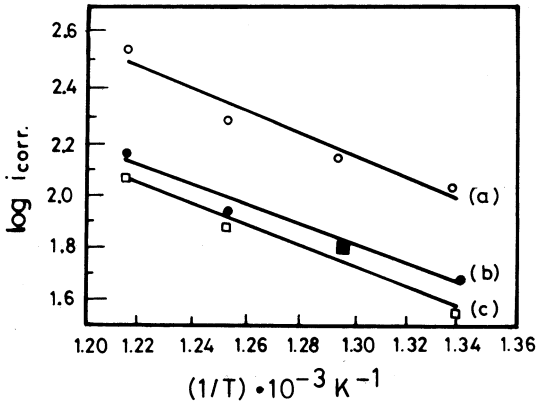

Fig. 1. (a–c) Arrhenius plots log i_{corr} vs. $1/T$ for stainless steel alloys SI (a), SII (b), SIII (c).

presented collectively in Fig. 1. The calculated values of the activation energy are 71.5, 74.1 and 70.7 kJ mol^{-1} for SI, SII and SIII, respectively. It is clear that the value of the activation energy is about the same which means that the mechanism of the corresponding passivation process is the same for the three investigated alloys.

3.2. Cyclic voltammetric measurements

To explain the corrosion and passivation behavior of the three investigated alloys it was essential to record the cyclic voltammograms of the three alloys in the melt. These measurements were carried out at 500 °C, and the potential was scanned between −2.0 and 0.0 V with a scan rate of 25 mV s^{-1}. this potential range is more negative than the open-circuit potential (i.e. the passivation potential, E_{pn}) of any of the investigated steel alloys at this temperature and more positive than the passivity breakdown potential, E_b, of each alloy. The cyclovoltammograms of SI, SII and SIII are presented in Fig. 2a–c, respectively. The results of these experiments are similar to those reported earlier for stainless steel alloys [5,7].

It is clear from Fig. 2 that the behavior of the austenitic steel specimens is about the same. The behavior of the ferritic steel is quite different (compare Fig. 2a with b and c). The cyclovoltammetric behavior of the alloys can be explained in the following way:

1) Starting at −2000 mV, the current increases gradually and peak A appears at ∼ −1850 mV. This peak can be attributed to the formation of $LiCrO_2$ according to reaction (1). This reaction corresponding to the dissolution of Cr under the formation of $LiCrO_2$ which passivates the surface and hence a decrease in the current is recorded. At more positive potential ∼ −1700 mV, a small peak B appears which may be ascribed to the oxidation of carbon by the oxygen ions coming from the carbonate decomposition (reaction 11) according to:

$$C + 3O^{2-} \rightarrow CO_3^{2-} + 4e \quad (15)$$

2) At potentials more positive than −1600 mV the oxidation of Fe occurs and peak C appears. This corresponds to reactions (2) and (3). The peak current density is dependent on the type of the steel. It is higher for steels with lower base metal content and hence it is higher for SIII followed by SII then SI.
3) At potentials of ∼ −1300 mV a broad peak, D, which corresponds to the formation of α-$LiFe_5O_8$ phase [6,12] presented by reaction (8), is recorded. In the case of austenitic steel alloys SII and SIII, nickel is contributing to the corrosion/passivation behavior and NiO is formed on the alloy surface (reaction (10)). The peak current density of peak D is relatively low, which confirm the increased passivity of this type of steel.
4) At more positive potentials ∼ −500 mV a peak or shoulder, peak E, is recorded. This peak is due to the further oxidation of FeO to α-Fe_2O_3 according to reactions (4) and (5) or the direct oxidation of Fe with oxygen ions according to reaction (9). In austenitic steel, the nickel oxidation contributes to this peak and higher nickel oxides are formed.

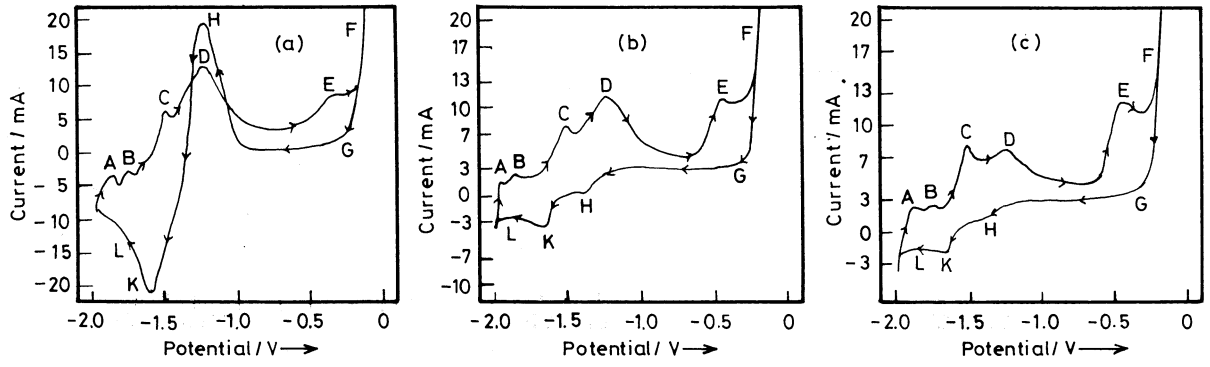

Fig. 2. (a–c) Cyclic voltammograms of stainless steel alloys SI (a), SII (b), SIII (c), in molten carbonate mixture at 500 °C using a scan rate of 25 mV s^{-1}.

$$2NiO + O^{2-} \rightarrow Ni_2O_3 + 2e \quad (16)$$

5) At potentials more than −200 mV, anodic oxidation of CO_3^{2-} with the evolution of oxygen and CO_2 according to reaction (12) takes place. This is accompanied by a large increase in the current density at peak F since the whole medium consists of CO_3^{2-}. The evolution of gas bubbles was observed at the anode with naked eyes.

On reversing the scan in the cathodic direction, the following cathodic reduction reactions can be considered.

1) At ∼−200 mV, the reduction of the accumulated gases to CO_3^{2-} takes place according to [the reverse of reaction (12):]
2) In austenitic steels (Fig. 3b,c) the cathodic scan shows small peaks (H & K) at potential ∼−1200 mV and ∼−1600 mV at which the reduction of Ni^{3+} to Ni^{2+} is to be considered. At more cathodic potentials the possibility of reduction of $LiFeO_2$ in the potential range −1600 to −1900 mV is considered. The peak L corresponds to the reduction of any Fe^{2+} to Fe. This reduction process may lead to:

$$LiFeO_2 + 3e \rightarrow Fe + Li^+ + 2O^{2-} \quad (17)$$

$$Fe^{2+} + 2e \rightarrow Fe \quad (18)$$

The oxygen ions remain in the melt and react with CO_2 leading to the formation of CO_3^{2-}. The cathodic behavior of ferritic steel alloy, SI, (cf. Fig. 2a) is quite different. At −900 mV the current increases sharply and peak H appears. This current increase, peak H, is a result of passivity breakdown due to cracking or spallation of the scale because of a reduction reaction of the form:

$$LiFe_5O_8 + 4e \rightarrow LiFeO_2 + 4FeO + 2O^{2-} \quad (19)$$

The formed FeO undergoes oxidation to $LiFeO_2$ and Fe_2O_3

$$FeO + Li^+ + O^{2-} \rightarrow LiFeO_2 + e \quad (20)$$

$$2FeO + O^{2-} \rightarrow Fe_2O_3 + 2e \quad (21)$$

The formation of the stable $LiFeO_2$ and Fe_2O_3 leads to the observation of the anodic current at peak H of the ferritic steel. At more negative potentials the reduction of $LiFeO_2$ takes place and the corresponding reduction peak at ∼−1400 mV is recorded. The peak currents are dependent on the nature of the alloy, the passivation film formed on its surface in the carbonate melt and also on the scan rate. The dependence of the peak currents on the scan rate is illustrated on Fig. 3. In this figure, the cyclic voltammograms of specimen SI at 50, 75 and 100 mV s^{-1} are presented. Compared to Fig. 2a, it is clear that some peaks disappear on increasing the scan rate, e.g. the peak E which represents the formation of α-Fe_2O_3 disappears, since this reaction is relatively slow and the increase of the scan rate did not give the reaction enough time to take place. The same observation was also recorded for the austenitic steel samples.

3.3. Corrosion tests on the oxide scales

In this series of experiments the stability of the anodically passivated stainless steel alloys in the carbonate melt was investigated in a corrosive medium. The working steel electrodes were anodically polarized in the carbonate melt at two different temperatures namely, 500 and 550 °C until it reaches the oxygen evolution stage, i.e. from −1300 to −100 mV, where the carbonate decomposition took place. The electrodes were removed from the melt, cooled, cleaned in the normal way and immersed in 0.2 M hydrochloric acid, (HCl), solution then the open-circuit potential was traced with time. Fig. 4(a–c) represents the open-circuit potential behavior of the three investigated alloys SI, SII, SIII, respectively.

It is clear from this figure that the open-circuit potential of the electrode measured at room temperature in 0.2 M HCl gets more negative with time in the first few minutes until it reaches a steady-state. In the case of

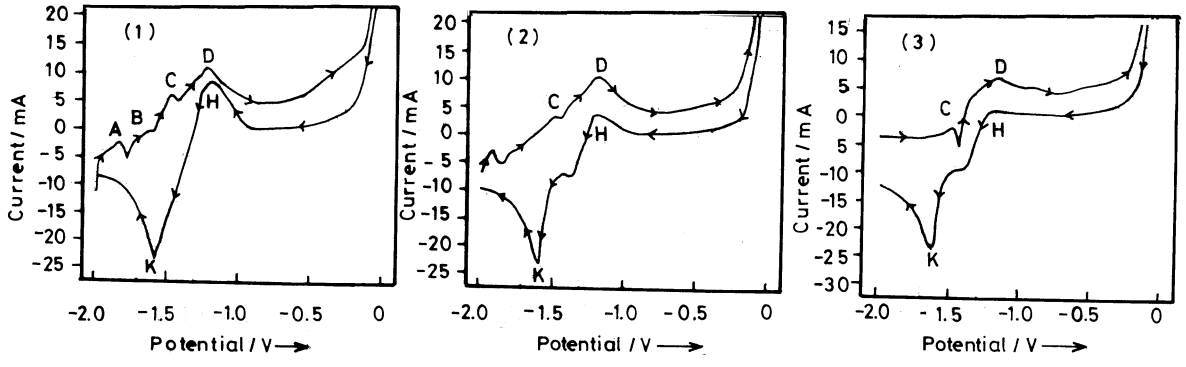

Fig. 3. Cyclic voltammograms of stainless steel alloy SI in molten carbonate mixture at 500 °C and different scan rates: (1) 50 mV s^{-1} (2) 75 mV s^{-1} (3) 100 mV s^{-1}.

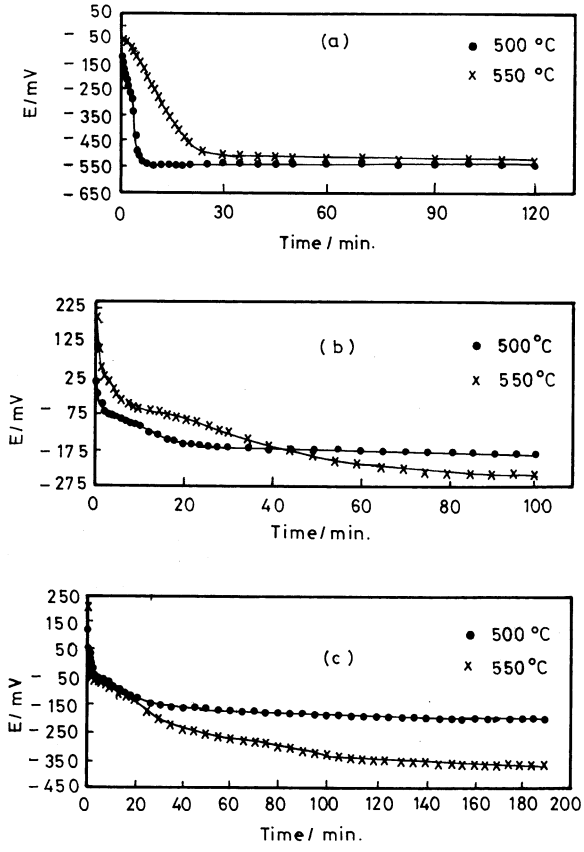

Fig. 4. (a–c) Potential vs. time curves of the a stainless steel alloys SI (a), SII (b), SIII (c), in 0.2 M HC after anodization in molten carbonate mixture at two different temperatures.

ferritic steel (SI) the immersion potential is less positive than that recorded for austenitic steel (SII, SIII). This indicates that the scale formed on the austenitic steel alloys is more passive than that formed on the ferritic alloy. At either temperature the steady-state potential of the ferritic steel alloy is not fluctuating, whereas the open-circuit potential of the austenitic steel alloys shows fluctuations and inflections. These inflections indicate the presence of a multilayered scale on the austenitic steel anodized surface, whereas the scales on the anodized ferritic steel alloy consist of single uniform layer.

The rate of scale dissolution may be calculated from the rate of variation of the difference in potential between the immerion potential, E_{imm}, and the steady-state potential, E_{ss}, expressed as mV min^{-1}. This value is directly proportional to the decrease in the scale thickness with time [21,22].

4. Conclusion

1) The anodic oxidation and scale formation on stainless steel in the carbonate melt occurs as a result of the electrochemical reactions taking place between the steel alloying elements and the carbonate melt.
2) The corrosion susceptibility of the austenitic steel alloys is less than that of the ferritic alloy.
3) The scales formed on austenitic steels are multilayered, whereas those formed on ferritic steels consist of a single uniform layer.

References

[1] J. Brounstein, G. Mamantov, G.P. Smith, Advances in Molten Salt Chemistry, Plenum Press, New York, 1971.
[2] W. Sundermeyer, Angew. Chem. 77 (1965) 241.
[3] T.B. Reddy, Electrochem. Technol. 1 (1963) 325.
[4] J.P.T. Vossen, L. Plomp, J.H.W. de Wit, J. Electrochem. Soc. 141 (1994) 340.
[5] J.P.T. Vossen, L. Plomp, J.H.W. de Wit, C. Rietveld, J. Electrochem. Soc. 142 (1995) 3327.
[6] J.P.T. Vossen, A.H.H. Janssen, J.H.W. de Wit, J. Electrochem. Soc. 143 (1996) 58.
[7] J.P.T. Vossen, P.C.H. Ament, J.H.W. de Wit, J. Electrochem. Soc. 143 (1996) 2272.
[8] C.G. Lee, H. Nakano, T. Nishina, I. Uchida, S. Kuroe, J. Electrochem. Soc. 145 (1998) 2747.
[9] N. Tatsuo, Y. Kohichi, U. Isamu, Proc. Electrochem. Soc. (1993), 93, Proceedings of the Third International Symposium on Carbonate Fuel Cell Technology, 1993, p. 264.
[10] R.B. Swaroop, J.W. Sim, K. Kinoshila, J. Electrochem. Soc. 125 (1978) 1799.
[11] R.A. Dando, L.G. Marianowski, H.C. Maru, J.R. Selman, J. Electrochem. Soc. 131 (1984) 2535, 2541.
[12] H. Yokokawa, N. Sakai, T. Kawada, M. Dokiya, J. Electrochem. Soc. 140 (1993) 3565.
[13] J.P.T. Vossen, R.C. Makkus, J.H.W. de Wit, J. Electrochem. Soc. 143 (1996) 66.
[14] H.H. Chamber, A.D.S. Tantram, in: G.Y. Young (Ed.), Fuel Cells, vol. 1, Reinhold, New York, 1960, pp. 94–108.
[15] S. Sendroff, A. Brenner, J. Electrochem. Soc. 101 (1954) 31.
[16] S.N. Flengas, E.K. Rideal, Proc. R. Soc. A 233 (1956) 443.
[17] S.N. Flengas, T.R. Ingraham, Can. J. Chem. 35 (1957) 1139.
[18] S.A. Salih, A.N. El-Masri, A.M. Baraka, J. Mater. Sci. 36 (2001) 1.
[19] W.A. Badawy, S.S. El-Egamy, Kh.M. Ismail, Br. Corros. J. 28 (1993) 133.
[20] P.W. Atkins, Physical Chemistry, 5th ed., Oxford University Press, Oxford, 1994, p. 877.
[21] W.M. Carrol, C.B. Berslin, Br. Corros. J. 26 (1991) 225.
[22] W.A. Badawy, F.M. Alkharafi, E.Y. Al-Hassan, Corros. Prevention Control 46 (1999) 51.